Optical Materials 72 (2017) 359–366

Contents lists available at ScienceDirect

Optical Materials

journal homepage: www.elsevier.com/locate/optmat

# Effect of Mg co-doping on cathodoluminescence properties of LuGAGG:Ce single crystalline garnet films

P. Schauer [a, *], O. Lalinský [a], M. Kučera [b], Z. Lučeničová [b], M. Hanuš [b]

[a] Institute of Scientific Instruments of the CAS, Královopolská 147, 612 64 Brno, Czech Republic
[b] Charles University, Faculty of Mathematics and Physics, 121 16 Prague, Czech Republic

ARTICLE INFO

*Article history:*
Received 12 April 2017
Received in revised form
13 June 2017
Accepted 14 June 2017

*Keywords:*
Multicomponent garnet film
LuGAGG:Ce,Mg
Liquid phase epitaxy
Cathodoluminescence
Scintillator
Electron detector

ABSTRACT

$Mg^{2+}$ co-doped $(LuGd)_3(GaAl)_5O_{12}$:Ce (LuGAGG:Ce,Mg) multicomponent single crystalline epitaxial garnet films were prepared and their cathodoluminescence (CL) and thermoluminescence (TSL) properties were studied in this paper. The films were prepared using the liquid phase epitaxy from lead-free $BaO$-$B_2O_3$-$BaF_2$ flux and their scintillation properties were characterized using the 10 keV collimated e-beam. More specifically, temperature dependent CL intensity, CL emission spectra, CL decay characteristics as well as TSL emission characteristics of the mentioned films were measured. At the highest content of Mg (700 ppm), the CL decay time was as low as 28 ns and the CL afterglow was as low as 0.01% at 1 μs after the e-beam excitation cut-off, which are important parameters for electron detectors in e-beam devices. The CL temperature quenching of the studied films began above room temperature. An increase of Mg concentration to or above 280 ppm quenched the characteristic CL emission of LuGAGG:Ce,Mg. The TSL measurements show that the trap population in studied garnet samples is considerably suppressed. The LuGAGG:Ce,Mg multicomponent single crystalline epitaxial films were evaluated as the perspective fast scintillators for the electron detectors in the e-beam devices.



## 1. Introduction

Most electron beam (e-beam) devices require a high-quality electron detector. Such an electron detector must primarily be very fast to process a large number of imaging or inspection data in real time. For example, for the acquisition of a high-quality image in a scanning electron microscope (SEM) in real time, it is usually required to process each pixel in less than 100 ns without a loss of contrast [1]. A much faster response of the electron detector is required for e-beam inspection systems [2,3], where the processing time for individual data must not exceed 10 ns, and there are requests from developers for a time of 1 ns or less. If the mentioned electron detectors are to be formed by scintillation detection systems, they must be equipped with very fast scintillators having a short decay time (decay to 1/*e* value, where *e* is the base of natural logarithms) and low afterglow even at a microsecond time range after an excitation cut-off. The scintillator with the long decay time causes an image blur and the scintillator with the high afterglow reduces image contrast in the SEM. As discussed [1], a dwell time of 50 ns (time for the single-pixel imaging) is required for the high-quality SEM image at the fast scanning. Using the results of the mentioned paper it is possible to assume that it is necessary to apply the scintillator with a decay time shorter than 40 ns and the afterglow lower than 0.1% in the microsecond time range to achieve satisfactory image contrast without the blurring for the dwell time of 50 ns. If the slow scintillator is used in the e-beam inspection system, it is not possible to perform real-time diagnostics.

It is generally known that organic (plastic) scintillators have the fastest response. In addition, these scintillators are technologically easy mastered and therefore cheap. Unfortunately, the plastic scintillators suffer from a strong degradation under the e-beams [4]. So their life is very short and there are mostly unusable for the electron detectors. On the contrary, inorganic scintillators have a higher resistance to the e-beam, and the Ce doped ones exhibit the relatively fast response. However, if they are to be resistant to radiation damage, the preparation of many of them is technologically demanding [5]. So many resistant inorganic scintillators are inaccessible and therefore expensive. Technologically more feasible are the inorganic scintillators with a garnet structure. This is a benefit to use the garnets in the electron detectors.

A new group of fast and high efficient scintillators based on

* Corresponding author.
*E-mail address:* petr@isibrno.cz (P. Schauer).

http://dx.doi.org/10.1016/j.optmat.2017.06.028
0925-3467/

cerium-activated multicomponent GAGG garnets has recently been reported [6–16]. Above all, the studies describing optical properties including the photoluminescence of GAGG:Ce are very promising. However, these studies provide only partial information for the use of these materials in the e-beam devices. In the electron detectors of these devices, the generation of photons takes place only in the surface layer of the scintillator (order of units of μm). Cathodoluminescence (CL) properties should be studied for such applications.

In the scintillation electron detectors, Czochralski grown single-crystal scintillators such as $Y_3Al_5O_{12}$:Ce (YAG:Ce) and $YAlO_3$:Ce (YAP:Ce), whose CL properties have been thoroughly studied [4,17–20], are commonly used today. A disadvantage of most of these single-crystal scintillators is their relatively long scintillation decay time (even longer than 100 ns for the YAG:Ce) and especially their high afterglow sometimes about 1%. The reason lies in the fact that in standard bulk single-crystal garnets, such as Czochralski grown YAG:Ce or LuAG:Ce, the shallow electron traps are responsible for the delayed radiative emission as well as for luminescence quenching [14,21–23]. Bulk single crystals of multicomponent garnets doped with cerium show a great improvement [11,12]. That is because the balanced Gd and Ga cations co-doping of these garnets suppresses the mentioned influence of shallow traps and prevents ionization-induced quenching of the $Ce^{3+}$ excited state. As a result, these multicomponent materials show significantly increased CL intensity near the estimated limit of garnet scintillators [23,24]. This suppression of shallow traps also has a positive influence on the decay characteristics including substantial reduction of the afterglow [25].

Besides the abovementioned bulk single-crystal scintillators, some of which are commonly used in the scintillation electron detectors in SEMs, the CL properties of very promising cerium activated multicomponent $(GdYLu)_3(GaAl)_5O_{12}$:Ce single crystalline epitaxial films [26] have recently been presented. The favorable CL properties of cerium activated single crystalline epitaxial films of gadolinium aluminum gallium garnet $Gd_3Al_{5-x}Ga_xO_{12}$:Ce (GAGG:Ce) were demonstrated in the SEM scintillation electron detector [27]. These multicomponent garnets represent a prospective scintillation system thanks to their high light yield (reported values up to 58 000 and 70 000 photons/MeV in single crystals [11,16,28–33] and ceramics [34], respectively), fast scintillation decay with a decay time of 50–100 ns [11,15,16,28,32–37], and reduced afterglow [13,15,34]. However, such a decay time can still be too high to deal with very fast imaging and inspection processes in e-beam devices. Thus, new materials with faster decay and substantially reduced afterglow are sought. For this reason, the effect of Mg co-doping on the CL properties of the LuGAGG:Ce multicomponent single crystalline epitaxial films is studied in this paper.

Recently, the liquid phase epitaxy technique has been used for the growth of multicomponent $(GdYLu)_3(GaAl)_5O_{12}$:Ce garnet films [15,38–40]. A novel lead-free $BaO\text{-}B_2O_3\text{-}BaF_2$ flux provided high light yield garnet single crystalline films with substantially suppressed slow scintillation components and very low afterglow [15]. Application of such films was successfully demonstrated in the SEM scintillation detector [27]. It has been recently shown that co-doping with divalent $Mg^{2+}$ or $Ca^{2+}$ ions significantly improves scintillation properties of LuAG:Ce [41–43] and GAGG:Ce garnets [35,36,44,45]. It was demonstrated that $Ca^{2+}$ co-doping reduces the trapped charge population in the crystal matrix of LSO:Ce, YSO:Ce, and GSO:Ce orthosilicates [46,47] and thus reduces the slow components and suppresses afterglow. Furthermore, the divalent co-doping can stabilize part of cerium ions in the tetravalent $Ce^{4+}$ state as was evidenced by XANES experiments [42,48–50]. Blahuta et al. [49] suggested mechanism involving $Ce^{4+}$ participation in the scintillation process, but some groups have objections to his hypothesis [51]. The discussion on the mechanism has not been yet finished and further studies should be carried out.

In our previous work [35], we demonstrated substantial improvement of scintillation properties of multicomponent $(LuGd)_3(GaAl)_5O_{12}$:Ce,Mg epitaxial garnet films due to the $Mg^{2+}$ co-doping. This co-doping significantly and primarily improved the timing characteristics of the LuGAGG:Ce,Mg LPE-grown films. Specifically, the scintillation decay time under soft X-ray or alpha particle excitations was shortened down to 30 ns, the intensities of the slow scintillation components were appreciably reduced, and the afterglow of 0.04% is particularly low for a garnet scintillator, about two times better than the best values published so far.

In this work we extend our previous studies [35] of LuGAGG:Ce,Mg epitaxial films to e-beam excitation for the intended application in SEM and other e-beam devices. We focused here especially on the impact of co-doping with divalent $Mg^{2+}$ ions on the scintillation and timing properties. We also demonstrate significant acceleration of scintillation decay under e-beam excitation and considerable reduction of the afterglow in the Mg co-doped specimens.

## 2. Experimental

### 2.1. Crystalline film preparation

Epitaxial garnet films $(LuGd)_3(GaAl)_5O_{12}$:Ce,Mg (LuGAGG:Ce,Mg) with a constant Ce content of 1% and Mg content which varied from 0 to 700 ppm (related to Lu + Gd content), were grown in the Technology Laboratory of Charles University, Prague, by isothermal dipping liquid phase epitaxy (LPE). The films were grown from the $BaO\text{-}B_2O_3$ -$BaF_2$ flux and deposited onto (100) oriented $Gd_3Ga_3Al_2O_{12}$ (GGAG) Czochralski grown substrates of 13 mm in diameter. The details on the LPE technique and the film growth were reported elsewhere [52,53]. The film thicknesses, determined by weighing, were in the range from 15 to 17.7 μm. The $Mg^{2+}$ content in the stoichiometric formula $(Ce_{0.01}Lu_{0.27}Gd_{0.74})_{3-x}Mg_x(Ga_{2.48}Al_{2.46})O_{12}$ is $x = 0–0.002$ (0–700 ppm). The composition was determined by EPMA (electron probe micro-analysis), Mg content by the GDMS (glow discharge mass spectrometry). Specimen parameters are presented in Table 1. All LuGAGG:Ce,Mg films were grown under the same conditions and from the same melt, except for Mg co-doping, and at the same growth temperature of 1030 °C. This guarantees that the studied specimens have the same composition and crystal properties and differ only in Mg co-doping.

The studied 1LGM series does not contain an Mg undoped LuGAGG:Ce specimen. Its inclusion was dropped because the 1LGM3 specimen has extremely low Mg concentration of 7 ppm that is within the range of other accidental aliovalent impurities in the specimen. In other words, the specimen with Mg of 7 ppm exhibits the same CL properties as the Mg-undoped one. Thus, the 1LGM3 specimen can be considered as Mg undoped and has been preferred in the study on Mg co-doping. In addition, the 1LGM series studied here can be compared with our other series [26,27,54]. In particular, the 14LBC series [26], containing the CL study of the $(GdLuY)_3(GaAl)_5O_{12}$:Ce films, complements the study of presented CL properties of the Mg co-doped 1LGM series.

As a reference specimen the LuAG:Ce epitaxial film was used which was grown using the same technology as the LuGAGG:Ce,Mg films. However, the LuAG:Ce film was grown onto (111) oriented LuAG substrate at the temperature of 1020 °C.

In order to prevent the specimen surface from being electrically charged, as well as to conduct and measure an excitation current during CL characterization, each specimen was coated with a thin Al film with the thickness of 50 nm. The Al film also helps to

**Table 1**
Parameters of the studied 1LGM series of the LuGAGG:Ce,Mg multicomponent epitaxial films. The series of 1LGM specimens was grown under the same conditions having the same concentration of Ce, Gd and Ga, respectively. The basic parameters of the reference specimen of the LuAG:Ce epitaxial film are also included. The 1LGM series includes the $(Ce_{(x/3)}Lu_{0.27}Gd_{(y/3)})_{3-w}Mg_w(Ga_zAl_{2.46})O_{12}$ films, where x, y, z and w values are as tabulated. The thickness in column 2 means the epitaxial film thickness. The Mg concentration in ppm is related to Lu + Gd content.

| Sign | thickness (μm) | $x_{Ce}$ | $y_{Gd}$ | $z_{Ga}$ | $w_{Mg}$ | Mg conc. (ppm) | Substrate |
|---|---|---|---|---|---|---|---|
| 1LGM3 | 16.3 | 0.03 | 2.22 | 2.48 | $2 \times 10^{-5}$ | 7 | GAGG |
| 1LGM5 | 17.2 | 0.03 | 2.22 | 2.48 | $10 \times 10^{-5}$ | 35 | GAGG |
| 1LGM7 | 16.8 | 0.03 | 2.22 | 2.48 | $80 \times 10^{-5}$ | 280 | GAGG |
| 1LGM8 | 16.7 | 0.03 | 2.22 | 2.48 | $200 \times 10^{-5}$ | 700 | GAGG |
| LuAG:Ce | 12.3 | 0.03 | 0 | 0 | 0 | 0 | LuAG |

increase the optical reflectivity to improve CL photon collection. The Al coating was deposited in a radio-frequency (RF) sputtering unit with 150 mm cathodes in the RF mode. Reactive sputtering was performed in argon and argon-oxygen atmospheres, respectively. The argon and oxygen fluxes were regulated with high accuracy by mass-flow controllers. The thickness was tested and calibrated using the Talystep surface profilometer.

### 2.2. Reference single crystal specimens

BGO ($Bi_4Ge_3O_{12}$) and LuAG:Ce single crystals were used as reference specimens. Both reference single crystal scintillators were borrowed from the Luminescence Laboratory of the Department of Optical Crystals in the Institute of Physics at the Czech Academy of Sciences. The BGO single crystal was grown by the Bridgman method, while the LuAG:Ce one was grown by the Czochralski method. Both single crystal scintillators were machined into a disc shape with a diameter of 7 mm and a thickness of 0.5 mm. Like the epitaxial films, each single crystal was coated with the Al film with the thickness of 50 nm using the RF sputtering to ensure its electrical conductivity as well as its optical reflectivity.

### 2.3. Cathodoluminescence characterization

LuGAGG:Ce,Mg single crystalline films were studied using the equipment for the study of cathodoluminescence (CL) properties built in our laboratory in Brno [55]. With this instrument, schematically drawn in Fig. 1, a collimated e-beam of 10 keV excited the investigated specimen and the CL emission was collected by the light-guide from the opposite side of the specimen. Due to the small penetration depth of 10 keV electrons <1 μm [56] all energy is deposited in the film and the substrate is not excited. An e-beam current of 30 nA and a spot diameter of 2 mm were used at the continuous (unmodulated) mode.

The CL emission spectra were measured using the Horiba JY iHR 320 spectrometer equipped with the Hamamatsu R943-02 photomultiplier tube (PMT). The CL spectra were corrected for the spectral response of the apparatus. To study CL decay, the e-beam was periodically deflected out of an aperture in order to create e-beam pulses with the repetition rate of 1 kHz and the pulse width of 50 ns. At pulsed mode the e-beam current pulse of 150 nA and the beam spot diameter of 2 mm were used. To study spectrally unresolved decay, instead of guiding the emitted light to the spectrometer, the light was directed to the ET-Enterprises 9113WB PMT connected to the Tektronix DPO7254 oscilloscope. Spectrally unresolved CL decays were measured in the whole spectral region between 200 and 800 nm. Using this setup a relative intensity of the CL emission was measured as a spectrally corrected PMT anode current.

The device for the CL characterization was equipped with a temperature-controlled specimen holder for measurements in the range from 100 K to 500 K. The desired specimen temperature was automatically stabilized using a PID controller [55].

### 2.4. Thermoluminescence characterization

A thermoluminescence (TSL) was taken after cooling the

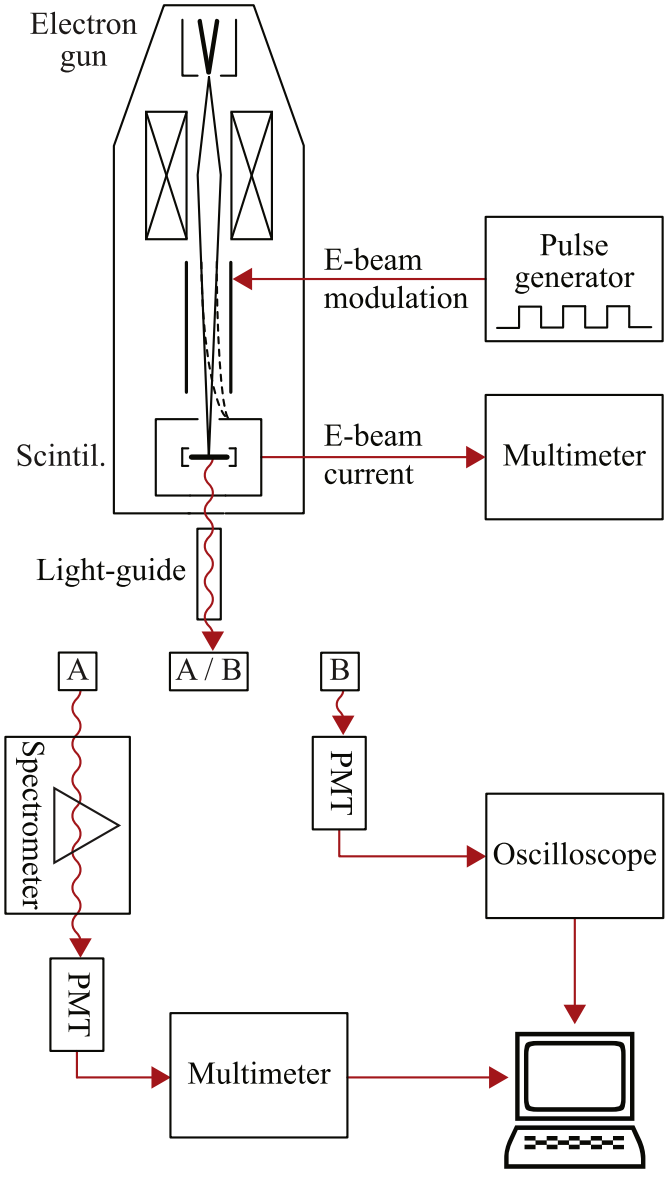


**Fig. 1.** Block diagram of the equipment for CL characterization of solids. The CL emission spectra were measured in unmodulated mode using the path A. The spectrally unresolved CL decays were measured in pulsed mode using the path B. Replacing an oscilloscope by a multimeter in the path B the CL intensity and the thermoluminescence were measured in unmodulated mode.

specimen down to 100 K. At this temperature the specimen was irradiated using the 10 keV e-beam with the current of 50 nA for 5 min. Thereafter the specimen was heated with the constant rate of 2 K $min^{-1}$. The spectrally unresolved CL emission (200–800 nm) was detected and TSL peaks were registered. During the TSL measurement, it is necessary to maintain the linear rate of the heat flow to the specimen. In this case, the tangential slope of the temperature trend was calculated and the PID controller kept its constant value.

## 3. Results and discussion

### 3.1. Cathodoluminescence emission spectroscopy

The CL emission spectra of Mg co-doped multicomponent epitaxial films LuGAGG:Ce with different Mg concentration are shown in Fig. 2. For comparison, also CL spectra of LuAG:Ce single crystal and of BGO single crystal are included. The spectra were measured in the wavelength range from 200 to 800 nm at room temperature, and subsequently they were corrected for the device spectral transmittance and also for the detector spectral sensitivity. Only $Ce^{3+}$-related 5d-4f emission is observed in the CL spectra of the studied epitaxial films in Fig. 2. The LuGAGG:Ce,Mg films have their CL emission maxima at about 548 nm, while the LuAG:Ce and BGO have their maxima in slightly lower spectral region at 507 nm and 487 nm, respectively. The maximum of the CL emission in the LuGAGG:Ce,Mg specimens is shifted towards lower energies (longer wavelengths) due to the Gd and Ga substitutions [11].

Regarding the dependency of characteristic CL intensity of LuGAGG:Ce,Mg on the Mg concentration, it is important to note that the CL intensity slightly increases with the Mg concentration, increasing up to tens of ppm. However, a further increase of Mg co-doping above 280 ppm quenches the characteristic $Ce^{3+}$ emission.

The CL emission spectra of the LuGAGG:Ce,Mg epitaxial film with the highest Mg concentration of 700 ppm (1LGM8), measured at different temperatures, are shown in Fig. 3. Analogous temperature dependencies were observed also in other LuGAGG:Ce,Mg films (not shown here, for details see Fig. 4). The 1LGM8 specimen with the highest Mg concentration was selected for the temperature dependence presentation since it exhibits excellent CL decay, as will be shown and discussed later in this paper. The characteristic CL intensity remains constant almost at the same maximal value in the temperature range from 100 to about 300 K and begins to decline rapidly above 310 K. This phenomenon will be described in greater detail in the following paragraph.

In order to describe the processes of the CL thermal quenching of the Mg co-doped LuGAGG:Ce epitaxial films more appropriately, the dependence of the spectrally unresolved CL intensity on the temperature was measured as described in Section 2.3. The term spectrally unresolved CL intensity means the CL intensity integrated over the spectral region of 200–800 nm. Since only 5d-4f Ce emission occurs in the measured spectral region, the spectrally unresolved curves actually refer to the characteristic Ce emission. The results for different Mg concentrations in the range from 7 to 700 ppm are shown in Fig. 4. The temperature axis of the graph is plotted as 1/T so that the slopes at higher temperatures provide information about the activation energy. The experimental results in Fig. 4 are fitted with the function [48,57].

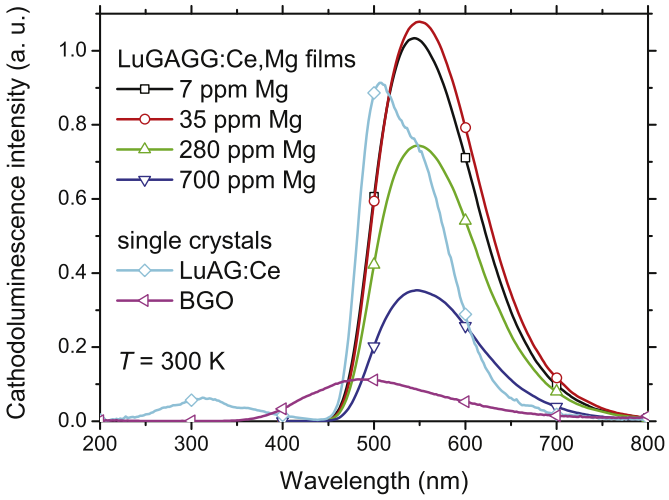


**Fig. 2.** The CL spectra of LuGAGG:Ce,Mg epitaxial films with various Mg concentration measured at room temperature. Reference $Bi_4Ge_3O_{12}$ (BGO) and LuAG:Ce single crystals are also shown for comparison.

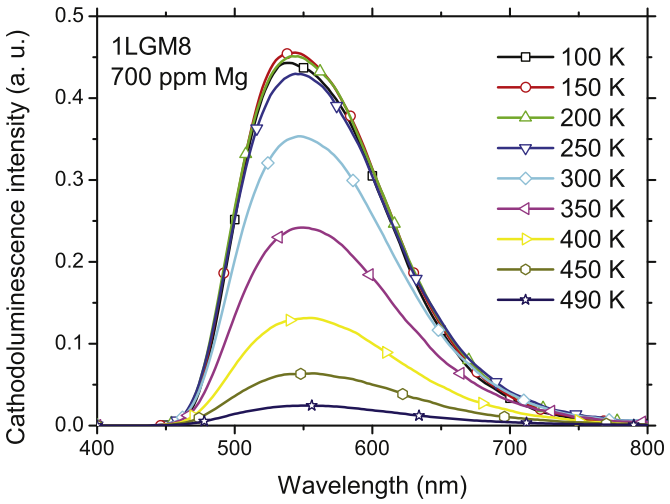


**Fig. 3.** The CL emission spectra of the LuGAGG:Ce,Mg epitaxial film with Mg concentration of 700 ppm (specimen 1LGM8) measured at different temperatures in the range of 100–490 K.

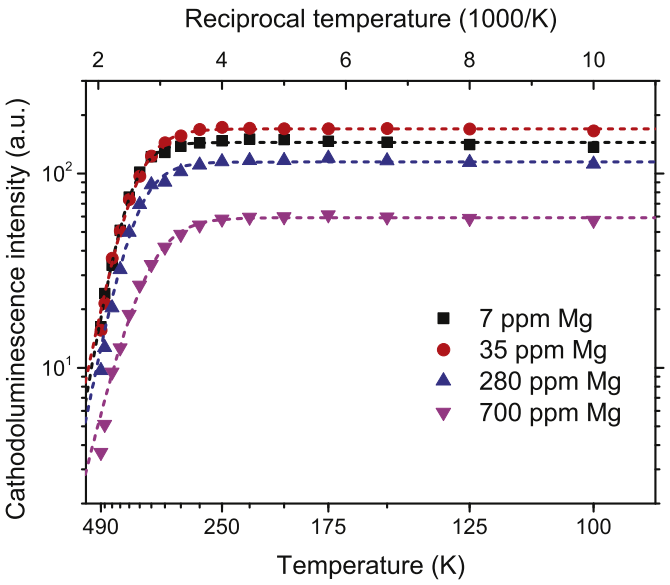


**Fig. 4.** Temperature dependence of the spectrally unresolved CL intensity of the LuGAGG:Ce,Mg epitaxial films. The dashed lines are fits using Equation (1), the fit parameters are summarized in Table 2.

$$I(T) = \frac{I_0}{1 + \xi \exp\left(-\frac{E_A}{k_B T}\right)} \quad (1)$$

where $I(T)$ is CL intensity at temperature $T$, $E_A$ is the activation energy related to the ionization and/or quenching process, $k_B$ is the Boltzmann constant, $I_0$ is the CL intensity at $T = 0$, and $\xi$ is the ratio of nonradiative to radiative transition probability.

For the studied LuGAGG:Ce,Mg epitaxial films the physical constants from Equation (1) were calculated, and the results are presented in Table 2. Like in the case of the CL emission spectra of the LuGAGG:Ce,Mg in Fig. 3, also spectrally unresolved CL intensity in Fig. 4 increases with Mg concentration increasing only for the concentrations up to tens of ppm, and the Mg concentration of 280 ppm causes only insignificant quenching of Ce emission. For all measured LuGAGG:Ce,Mg epitaxial films the thermal quenching begins in the temperature region from 310 to 380 K. For convenience, in Table 2 we also report temperature $T_Q$ when the CL intensity decreases to 90% of the low temperature value. It should be emphasized that the Mg co-doping doesn't have any appreciable impact on the thermal quenching.

### 3.2. Spectrally unresolved cathodoluminescence decay

The CL decay curves of the LuGAGG:Ce,Mg multicomponent epitaxial films with different Mg concentration, measured at room temperature, are shown in Fig. 5. The numerical values of decay time (decay to 1/e value) and of the afterglow at 1 μs after e-beam excitation cut off, read from the resulting graph in Fig. 5, are in Table 2. For comparison, the CL decay characteristic of the LuAG:Ce single crystal (SC) is also included. The results were corrected for the pulse width and for the instrument response function (IRF). In this paper, a fitting of the experimental decay curve is only a mathematical tool to present the smooth curve and consequently to determine the decay time and afterglow values. Fittings were carried out assuming the multi-exponential functions. This means that the curves presented are the result of the IRF and multi-exponential fit convolution.

The presented decay intensities were normalized to unity at the beginning of decay. Such a graphical representation with high dynamic range of decay intensities allows the determination of both the decay time (time when the intensity drop to $1/e$), and also other individual decay components of LuGAGG: Ce,Mg films, including the values of their afterglows in the microsecond region.

The LuGAGG:Ce,Mg films exhibit a decrease of their CL decay time from 61 ns to 28 ns with increased Mg co-doping from 7 ppm to 700 ppm. This implies that the response of the fast CL components gradually decreases with increasing concentration of $Mg^{2+}$ ions. Thus, high Mg co-doping of the LuGAGG:Ce,Mg films brings a significant improvement compared with LuAG:Ce single crystal that exhibits the decay time of 47 ns. More importantly, in the LuGAGG:Ce,Mg films the slow decay components are suppressed unlike the LuAG:Ce single crystal. As already expressed in introductory Section 1, in the scanning scintillation imaging systems of the e-beam devices the afterglow must be low even at the time by only one or two orders of magnitude higher than the decay time. Therefore, the measurement of the afterglow was carried out in the microsecond time region. The CL afterglow of the slightly co-doped (7 ppm of Mg) LuGAGG:Ce,Mg film (measured at 1 μs after e-beam excitation cut off) was only about 0.12% and even only about 0.01% for the highly co-doped (700 ppm of Mg) one, while the afterglow of the LuAG:Ce single crystal was as high as 2%.

Changes in the CL decay characteristics of the Mg co-doped (280 ppm of Mg) LuGAGG:Ce multicomponent epitaxial film at different temperatures are shown in Fig. 6. As in the previous figure, the presented decay intensities were corrected for the pulse width as well as for IRF, and curves were normalized to unity. Also in this

**Table 2**
The CL properties of the LuGAGG:Ce,Mg epitaxial films (specimens 1LGMx) compared with the LuAG:Ce single crystal (SC). $W_{Mg}$ is the concentration of Mg in ppm related to the Lu + Gd content, $\tau_e$ is the decay time (decay to $1/e$ value), $AG_{1\mu s}$ is the afterglow at 1 μs after e-beam excitation cut-off, $T_Q$ is the quenching temperature (at 90% of $I_0$). $I_0$ is the intensity at low temperatures in the constant region ($T < 200$ K), $\xi$ is the ratio of nonradiative to radiative transition probability, and $E_A$ is the activation energy related to the ionization and/or quenching process, as described in Equation (1).

| Sign | $W_{Mg}$ (ppm) | $\tau_e$ (ns) | $AG_{1\mu s}$ (%) | $I_0$ (a.u.) | $T_Q$ (K) | $\xi$ | $E_A$ (eV) |
|---|---|---|---|---|---|---|---|
| 1LGM3 | 7 | 61 | 0.12 | 145 | 380 | 52613 | 0,377 |
| 1LGM5 | 35 | 60 | 0.07 | 170 | 320 | 14010 | 0,317 |
| 1LGM7 | 280 | 48 | 0.04 | 115 | 350 | 18002 | 0,325 |
| 1LGM8 | 700 | 28 | 0.01 | 59.3 | 310 | 4660 | 0,262 |
| LuAG:Ce SC | 0 | 47 | 2 | n/a | n/a | n/a | n/a |

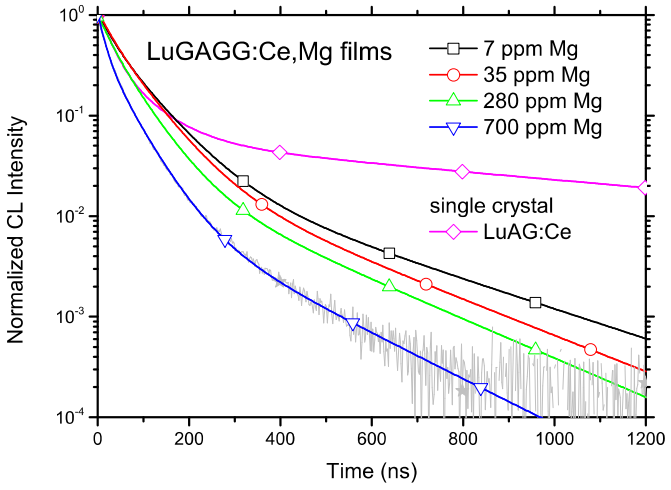


**Fig. 5.** Normalized spectrally unresolved CL decays of LuGAGG:Ce,Mg films with various Mg concentrations measured at room temperature under 50 ns e-beam excitation. Reference LuAG:Ce single crystal is also shown. The labeled smooth curves were obtained using multi-exponential fittings of measured decay. Measured decay (grey line) is shown only for the specimen 1LGM8 (700 ppm Mg) for clarity.

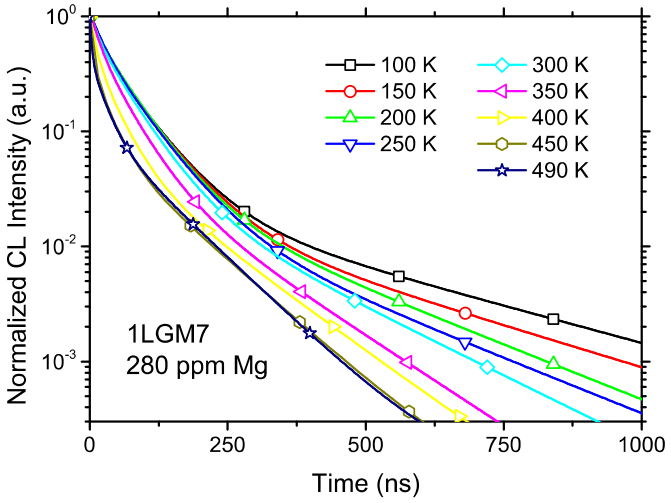


**Fig. 6.** Normalized spectrally unresolved CL decays of the LuGAGG:Ce,Mg film (1LGM7, 280 ppm of Mg) at different temperatures under 50 ns e-beam excitation. The curves represent multi-exponential fittings of measured decay.

case fittings were carried out using the multi-exponential function so that the curves represent the IRF and multi-exponential fit convolution. Compared to the previous figure, Fig. 6 shows results with a somewhat slower response, so a slightly reduced time axis range has been chosen to offer better interpretation of the results. It is seen that CL decay decreases monotonously with increasing temperature. As for the fast decay component, the decay time at 100 K is approximately 46 ns (and it does not change noticeably up to room temperature), while the decay time at 490 K is only approximately 8.6 ns. Even more significant is the decrease of the CL afterglow with increasing temperature. The afterglow (measured at 1 μs after e-beam excitation cut-off) is about 0.14% at 100 K, while it is below 0.001% (a value close to the background signal of the measuring device) at 490 K.

### 3.3. Thermoluminescence

Using the electron excitation of the specimen at a significantly reduced temperature to 100 K a thermoluminescence (TSL) of studied epitaxial films as well as of LuAG:Ce epitaxial film and single crystal was measured during the following heating up to 500 K. In materials that show TSL peaks electronic excited states are trapped or arrested for extended periods of time just by the localized defects or imperfections. Heating the material enables the trapped states to interact with phonons to rapidly decay into lower-energy states, causing the emission of photons in the process. Therefore the course of the TSL of the Mg co-doped (280 ppm of Mg) LuGAGG:Ce multicomponent epitaxial film, as well as that of the LuAG:Ce epitaxial film or single crystal, shown in Fig. 7, provide valuable information about the presence or absence of the mentioned localized defects or imperfections.

The advantage of electron excitation is the fact that TSL is not dependent on the specimen volume, but it is dependent on the electron interaction volume that is essentially the same for both bulk and film specimens. The mean free path of the interacting electrons is also almost the same for the both mentioned specimens. This allows us to compare specimens of different volumes.

It is seen that only the LuAG:Ce single crystal exhibits prominent TSL peaks. The epitaxial films show a very weak TSL signal, about two orders of magnitude weaker as compared to the reference single crystal. This allows an assessment of the presence of shallow traps and put this into context of the measurement of the CL spectral and decay characteristics.

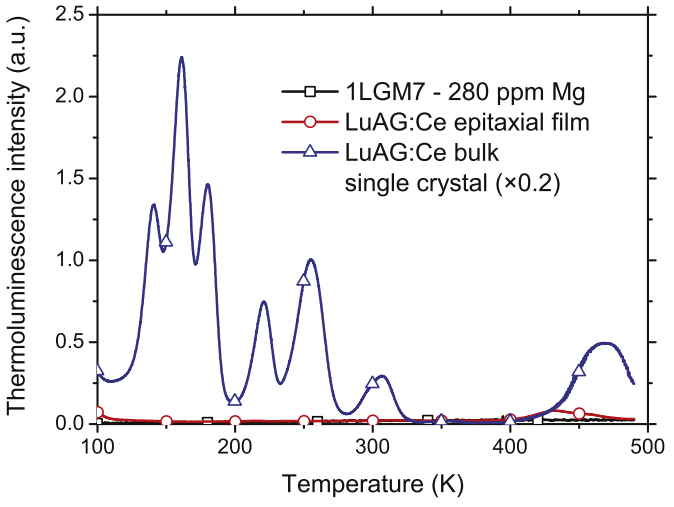


**Fig. 7.** Thermoluminescence (TSL) of the Mg co-doped (280 ppm of Mg) LuGAGG:Ce epitaxial film, LuAG:Ce epitaxial film and LuAG:Ce single crystal. The specimens were excited by e-beam for 5 min at 100 K and thereafter heated to 500 K with the constant rate of 2 K $min^{-1}$.

### 3.4. Discussion of results

The presented results of CL study of the LuGAGG:Ce,Mg multicomponent epitaxial films show that a strategy to get significantly faster CL decays and greatly suppressed afterglow in garnet scintillators by balanced co-doping with divalent ions is effective. The TSL measurements show that the trap population in studied samples is significantly suppressed. Although $Mg^{2+}$ co-doping of LuGAGG:Ce does not favorably affect the CL intensity presented in Figs. 2 and 4, the CL decay decreases significantly at higher $Mg^{2+}$ concentration, as presented in Fig. 5. Especially the afterglow at the microsecond time range is considerably suppressed, which is very important for very fast imaging and inspection processes in e-beam devices or in detectors operating at high-rate conditions, such as PET, SEM, or in colliders.

The temperature dependence of the CL intensity shows no increase with the temperature. It is fully in accordance with Equation (1). This implies that the CL mechanism doesn't contain thermally activated processes that would increase the probability of radiative transitions. The measured curves of temperature dependence correspond to the pure mechanism of the thermal quenching.

In terms of practical use, it is important that considerable CL temperature quenching of all the studied LuGAGG:Ce,Mg epitaxial films begins approximately at the temperature of 300 K, i.e. above room temperature. This quenching temperature depends on the host composition, first of all Ga/Al ratio, and it is not noticeably influenced by Mg co-doping as is evident from Fig. 4. The LuGAGG:Ce,Mg epitaxial film scintillators may be useful even in an environment with a considerably higher temperature, because they show at least 50% of the low temperature intensity up to the temperature of 400 K. Furthermore, the thermal quenching temperature can be substantially increased by decreasing Ga/Al ratio. Equally important is considerable improvement of the CL kinetics. The results in Fig. 5 show significant shortening of the CL decay time to approximately 28 ns for the LuGAGG:Ce,Mg epitaxial film (specimen 1LGM8 with $Mg^{2+}$ content of 700 ppm) as compared with approximately 60 ns for GAGG:Ce. Although this is at the expense of the CL intensity, this specimen has still comparable CL intensity with that of YAG:Ce. Moreover, the particularly low CL afterglow (0.01% at 1μs and 0.005% at 2 μs after e-beam excitation cut off) of the mentioned LuGAGG:Ce,Mg specimen is by far the best value ever reported for garnets. So the positive effect of $Mg^{2+}$ co-doping is evident.

Another major positive feature of the presented LuGAGG:Ce,Mg multicomponent epitaxial films is their different preparation technology compared with the standard bulk single crystal garnets. Unfortunately, Czochralski grown single-crystal garnets possess antisite defects that are responsible for the broad UV emission at 250–400 nm in Fig. 2, as well as for the slow CL decay components and associated high afterglow in the microsecond time range in Fig. 5. Moreover, Czochralski grown garnets have the shallow electron traps that are responsible for the dominant TSL peaks in Fig. 7. The developers of scintillation electron detectors have dealt with this problem for many years [20,58]. The lower preparation temperatures during the growth process are the main causes of the antisite defects absence in the epitaxial films, as demonstrated on the thermoluminescence curves in Fig. 7. Furthermore, in order to modify the Czochralski grown single-crystal garnets into a suitable scintillator size and/or shape, operations such as cutting, grinding, and polishing must be accomplished, which is a significant encroachment on the properties of their surface [20]. However, in the electron detector, relevant CL phenomena take place in the

surface layer not thicker than some μm. No finishing is required with epitaxial layers, because they are already grown on the prepared size and shape of the substrate. Therefore, the scintillation properties of epitaxial film surfaces are not adversely affected by additional treatment.

## 4. Conclusion

To perform real-time diagnostics with the e-beam instruments, new scintillators for electron detectors with faster decay were sought resulting in the preparation and CL study of the Mg co-doped $(LuGd)_3(GaAl)_5O_{12}$:Ce,Mg (LuGAGG:Ce,Mg) multicomponent single crystalline epitaxial films specified in Section 2.1. The films were prepared using the epitaxial growth from lead-free BaO-$B_2O_3$-$BaF_2$ flux onto (100) oriented GGAG Czochralski grown substrates, and subsequently the Al film with a thickness of 50 nm was sputtered on their surfaces. These specimens were characterized using the cathodoluminescence (CL) and thermoluminescence (TSL) excited by the 10 keV collimated e-beam. More specifically, temperature dependent CL intensity, CL emission spectra, CL decay, as well as TSL emission of the mentioned film scintillators were measured and interpreted to get their scintillation parameters.

The presented CL study of LuGAGG:Ce,Mg films shows that a balanced Mg-Gd-Ga admixture into the LuAG:Ce films provided excellent scintillators for electron detectors. In such scintillators, the effect of unwanted potential traps is suppressed as demonstrated in TSL measurements. The observed CL decay time is only about 28 ns, and the CL afterglow at 1 μs after e-beam excitation cut-off is as low as 0.01% for the highest content of Mg (700 ppm), which is very important for electron detectors in e-beam devices. From practical point of view, it is important that considerable CL temperature quenching of studied epitaxial films begins above room temperature. Another advantage of the LuGAGG:Ce,Mg multicomponent epitaxial films studied lies in different conditions of the growth technology, characterized by the lower preparation temperatures, resulting in the antisite defect absence. Furthermore, the scintillation properties of the studied epitaxial films are not deteriorated by an additional mechanical and/or chemical finishing of their surfaces. On the other hand, it should be mentioned that the CL intensity of LuGAGG:Ce,Mg films slightly increases with increasing Mg concentration only for the concentration up to tens of ppm. A further increase of Mg co-doping above 100 ppm quenches the characteristic CL emission of the LuGAGG:Ce,Mg. Compared with the photoluminescence study, which is a result of a photon interaction in a subsurface volume [54], the CL study of LuGAGG:Ce,Mg films confirmed that the film surfaces, characterized in this paper, have essentially the same properties as the subsurface volume.

Especially fast enough response predetermines the LuGAGG:-Ce,Mg multicomponent single crystalline epitaxial films as the perspective fast scintillators for the electron detectors in e-beam devices where a somewhat reduced intensity can be expendable.

## Acknowledgement

The research was supported by the Czech Science Foundation (project, GA16-05631S and GA16-15569S) and by the Ministry of Education, Youth and Sports of the Czech Republic (project LO1212). The research infrastructure was funded by the Ministry of Education, Youth and Sports of the Czech Republic and the European Commission (project CZ.1.05/2.1.00/01.0017).

## References

[1] J. Bok, P. Schauer, Performance of SEM scintillation detector evaluated by modulation transfer function and detective quantum efficiency function, Scanning 36 (2014) 384–393.
[2] T. Hirano, S. Yamaguchi, M. Naka, M. Itoh, M. Kadowaki, T. Koike, Y. Yamazaki, K. Terao, M. Hatakeyama, H. Sobukawa, Development of EB inspection system EBeyeM for EUV mask, in: M.W. Montgomery, W. Maurer (Eds.), SPIE Photomask Technology, International Society for Optics and Photonics, 2010, 2C-1–2C-8.
[3] O.D. Patterson, J. Lee, M.D. Monkowski, D.A. Ryan, S.-T. Chen, S.C. Lei, F. Wang, C.H. Lee, D. Tomlinson, W. Fang, E-beam inspection system for comparison of wafer and design data, in: A. Starikov (Ed.), SPIE Advanced Lithography, International Society for Optics and Photonics, 2012, 2J-1–2J-9.
[4] R. Autrata, P. Schauer, J. Kvapil, J. Kvapil, Single-crystal aluminates-a new generation of scintillators for scanning electron microscopes and transparent screens in electron optical devices, Scanning Electron Microsc. 2 (1983) 489.
[5] G.F. Knoll, Radiation Detection and Measurement, fourth ed., John Wiley, Hoboken, N.J., 2010.
[6] V. Babin, K. Chernenko, M. Kučera, M. Nikl, S. Zazubovich, Photostimulated luminescence and defects creation processes in $Ce^{3+}$-doped epitaxial films of multicomponent $Lu_{3-x}Gd_xGa_yAl_{5-y}O_{12}$ garnets, J. Luminescence 179 (2016) 487–495.
[7] K. Bartosiewicz, V. Babin, K. Kamada, A. Yoshikawa, J. Mares, A. Beitlerova, M. Nikl, Luminescence quenching and scintillation response in the $Ce^{3+}$ doped $Gd_xY_{3-x}Al_5O_{12}$ (x = 0.75, 1, 1.25, 1.5, 1.75, 2) single crystals, Opt. Mater. 63 (2017) 134–142.
[8] K. Bartosiewicz, V. Babin, K. Kamada, A. Yoshikawa, M. Nikl, Energy migration processes in undoped and Ce-doped multicomponent garnet single crystal scintillators, J. Luminescence 166 (2015) 117–122.
[9] K. Brylew, W. Drozdowski, A.J. Wojtowicz, K. Kamada, A. Yoshikawa, Studies of low temperature thermoluminescence of GAGG: Ce and LuAG: Pr scintillator crystals using the T max–T stop method, J. Luminescence 154 (2014) 452–457.
[10] W. Chewpraditkul, P. Brůža, D. Pánek, N. Pattanaboonmee, K. Wantong, W. Chewpraditkul, V. Babin, K. Bartosiewicz, K. Kamada, A. Yoshikawa, Optical and scintillation properties of $Ce^{3+}$-doped $YGd_2Al_{5-x}Ga_xO_{12}$ (x = 2, 3, 4) single crystal scintillators, J. Luminescence 169 (2016) 43–50.
[11] K. Kamada, T. Endo, K. Tsutumi, T. Yanagida, Y. Fujimoto, A. Fukabori, A. Yoshikawa, J. Pejchal, M. Nikl, Composition engineering in cerium-doped (Lu, Gd) 3 (Ga, Al) $5O_{12}$ single-crystal scintillators, Cryst. Growth Des. 11 (2011) 4484–4490.
[12] K. Kamada, T. Yanagida, J. Pejchal, M. Nikl, T. Endo, K. Tsutumi, Y. Fujimoto, A. Fukabori, A. Yoshikawa, Scintillator-oriented combinatorial search in Ce-doped (Y, Gd) 3 (Ga, Al) $5O_{12}$ multicomponent garnet compounds, J. Phys. D Appl. Phys. 44 (2011) 505104.
[13] E. Mihóková, K. Vávrů, K. Kamada, V. Babin, A. Yoshikawa, M. Nikl, Deep trapping states in cerium doped (Lu, Y, Gd) 3 (Ga, Al) 5 $O_{12}$ single crystal scintillators, Radiat. Meas. 56 (2013) 98–101.
[14] M. Nikl, A. Yoshikawa, Recent R&D trends in inorganic single-crystal scintillator materials for radiation detection, Adv. Opt. Mater. 3 (2015) 463–481.
[15] P. Prusa, M. Kucera, J.A. Mares, Z. Onderisinova, M. Hanus, V. Babin, A. Beitlerova, M. Nikl, Composition tailoring in Ce-doped multicomponent garnet epitaxial film scintillators, Cryst. Growth Des. 15 (2015) 3715–3723.
[16] K. Kamada, T. Yanagida, T. Endo, K. Tsutumi, Y. Usuki, M. Nikl, Y. Fujimoto, A. Fukabori, A. Yoshikawa, 2inch diameter single crystal growth and scintillation properties of Ce: $Gd_3Al_2Ga_3O_{12}$, J. Cryst. Growth 352 (2012) 88–90.
[17] R. Autrata, P. Schauer, J. Kvapil, J. Kvapil, A single crystal of YAG-new fast scintillator in SEM, J. Phys. E Sci. Instrum. 11 (1978) 707.
[18] R. Autrata, P. Schauer, J. Kvapil, J. Kvapil, A single crystal of $YAlO_3$: $Ce^{3+}$ as a fast scintillator in SEM, Scanning 5 (1983) 91–96.
[19] R. Autrata, P. Schauer, J. Kvapil, J. Kvapil, Cathodoluminescent efficiency of $Y_3Al_5O_{12}$ and $YAlO_3$ single crystals in dependence on $Ce^{3+}$ and other dopants concentration, Cryst. Res. Technol. 18 (1983) 907–913.
[20] P. Schauer, Optimization of decay kinetics of YAG: Ce single crystal scintillators for S (T) EM electron detectors, Nucl. Instrum. Methods Phys. Res. Sect. B Beam Interact. Mater. Atoms 269 (2011) 2572–2577.
[21] M. Nikl, A. Vedda, M. Fasoli, I. Fontana, V. Laguta, E. Mihokova, J. Pejchal, J. Rosa, K. Nejezchleb, Shallow traps and radiative recombination processes in $Lu_3Al_5O_{12}$: Ce single crystal scintillator, Phys. Rev. B 76 (2007) 195121.
[22] W. Chewpraditkul, L. Swiderski, M. Moszynski, T. Szczesniak, A. Syntfeld-Kazuch, C. Wanarak, P. Limsuwan, Scintillation properties of LuAG: Ce, YAG: Ce and LYSO: Ce crystals for gamma-ray detection, IEEE Trans. Nucl. Sci. 56 (2009) 3800–3805.
[23] M. Nikl, A. Yoshikawa, K. Kamada, K. Nejezchleb, C. Stanek, J. Mares, K. Blazek, Development of LuAG-based scintillator crystals–a review, Prog. Cryst. Growth Charact. Mater. 59 (2013) 47–72.
[24] P. Dorenbos, Fundamental limitations in the performance of $Ce^{3+}$-, $Pr^{3+}$-, and $Eu^{2+}$-Activated scintillators, IEEE Trans. Nucl. Sci. 57 (2010) 1162–1167.
[25] M. Nikl, K. Kamada, V. Babin, J. Pejchal, K. Pilarova, E. Mihokova, A. Beitlerova, K. Bartosiewicz, S. Kurosawa, A. Yoshikawa, Defect engineering in Ce-doped aluminum garnet single crystal scintillators, Cryst. Growth Des. 14 (2014) 4827–4833.
[26] M. Kucera, Z. Onderisinova, J. Bok, M. Hanus, P. Schauer, M. Nikl, Scintillation response of $Ce^{3+}$ doped GdGa-LuAG multicomponent garnet films under e-beam excitation, J. Luminescence 169 (2016) 674–677.
[27] J. Bok, O. Lalinský, M. Hanuš, Z. Onderišinová, J. Kelar, M. Kučera, GAGG: ce single crystalline films: new perspective scintillators for electron detection in

SEM, Ultramicroscopy 163 (2016) 1–5.
[28] K. Kamada, S. Kurosawa, P. Prusa, M. Nikl, V.V. Kochurikhin, T. Endo, K. Tsutumi, H. Sato, Y. Yokota, K. Sugiyama, Cz grown 2-in. size Ce: $Gd_3$ (Al, Ga) 5 $O_{12}$ single crystal; relationship between Al, Ga site occupancy and scintillation properties, Opt. Mater. 36 (2014) 1942–1945.
[29] N.J. Cherepy, S.A. Payne, B.W. Sturm, J.D. Kuntz, Z.M. Seeley, B.L. Rupert, R.D. Sanner, O.B. Drury, T.A. Hurst, S.E. Fisher, M. Groza, L. Matei, A. Burger, R. Hawrami, K.S. Shah, L.A. Boatner, Comparative gamma spectroscopy with SrI2(Eu), GYGAG(Ce) and Bi-loaded plastic scintillators, Ieee Nucl. Sci. Conf. R. (2010) 1288–1291.
[30] N.J. Cherepy, Z.M. Seeley, S.A. Payne, P.R. Beck, O.B. Drury, S.P. O'Neal, K.M. Figueroa, S. Hunter, L. Ahle, P.A. Thelin, T. Stefanik, J. Kindem, Development of transparent ceramic Ce-doped gadolinium garnet gamma spectrometers, Ieee Trans. Nucl. Sci. 60 (2013) 2330–2335.
[31] N.J. Cherepy, Z.M. Seeley, S.A. Payne, P.R. Beck, E.L. Swanberg, S. Hunter, L. Ahle, S.E. Fisher, C. Melcher, H. Wei, T. Stefanik, Y.S. Chung, J. Kindem, High energy resolution transparent ceramic garnet scintillators, Proc. Spie 9213 (2014).
[32] F. Meng, M. Koschan, Y.T. Wu, C.L. Melcher, Relationship between $Ca^{2+}$ concentration and the properties of codoped $Gd_3Ga_3Al_2O_{12}$:Ce scintillators, Nucl. Instrum. Methods A 797 (2015) 138–143.
[33] M. Tyagi, F. Meng, M. Koschan, S.B. Donnald, H. Rothfuss, C.L. Melcher, Effect of codoping on scintillation and optical properties of a Ce-doped $Gd_3Ga_3Al_2O_{12}$ scintillator, J. Phys. D. Appl. Phys. 46 (2013).
[34] T. Yanagida, K. Kamada, Y. Fujimoto, H. Yagi, T. Yanagitani, Comparative study of ceramic and single crystal Ce:GAGG scintillator, Opt. Mater. 35 (2013) 2480–2485.
[35] P. Průša, M. Kučera, V. Babin, P. Brůža, D. Pánek, A. Beitlerová, J.A. Mareš, M. Hanuš, Z. Lučeničová, M. Nikl, Garnet scintillators of superior timing characteristics: material, engineering by liquid phase epitaxy, Adv. Opt. Mater. 5 (2017) 1600875.
[36] M. Lucchini, V. Babin, P. Bohacek, S. Gundacker, K. Kamada, M. Nikl, A. Petrosyan, A. Yoshikawa, E. Auffray, Effect of $Mg^{2+}$ ions co-doping on timing performance and radiation tolerance of cerium doped $Gd_3Al_2Ga_3O_{12}$ crystals, nuclear instruments and methods in Physics research section a: accelerators, spectrometers, Detect. Assoc. Equip. 816 (2016) 176–183.
[37] H. Yamaguchi, K. Kamada, S. Kurosawa, J. Pejchal, Y. Shoji, Y. Yokota, Y. Ohashi, A. Yoshikawa, Co-doping effects on luminescence and scintillation properties of Ce doped $(Lu, Gd)_3(Ga, Al)_5O_{12}$ scintillator, Opt. Mater. 61 (2016) 129–133.
[38] M. Kucera, M. Hanus, Z. Onderisinova, P. Prusa, A. Beitlerova, M. Nikl, Energy transfer and scintillation properties of doped multicomponent garnets, IEEE Trans. Nucl. Sci. 61 (2014) 282–289.
[39] P. Prusa, M. Kucera, J. Mares, M. Hanus, A. Beitlerova, Z. Onderisinova, M. Nikl, Scintillation properties of the Ce-doped multicomponent garnet epitaxial films, Opt. Mater. 35 (2013) 2444–2448.
[40] Y. Zorenko, V. Gorbenko, T. Zorenko, O. Sidletskiy, A. Fedorov, P. Bilski, A. Twardak, High-performance Ce-doped multicomponent garnet single crystalline film scintillators, Phys. Status Solidi (RRL)-Rapid Res. Lett. 9 (2015) 489–493.
[41] S. Liu, X. Feng, Z. Zhou, M. Nikl, Y. Shi, Y. Pan, Effect of $Mg^{2+}$ co-doping on the scintillation performance of LuAG: Ce ceramics, Phys. Status Solidi (RRL)-Rapid Res. Lett. 8 (2014) 105–109.
[42] S.P. Liu, J.A. Mares, X.Q. Feng, A. Vedda, M. Fasoli, Y. Shi, H.M. Kou, A. Beitlerova, L.X. Wu, C. D'Ambrosio, Y.B. Pan, M. Nikl, Towards bright and fast $Lu_3Al_5O_{12}$:Ce,Mg optical ceramics scintillators, Adv. Opt. Mater. 4 (2016) 731–739.
[43] K. Kamada, M. Nikl, S. Kurosawa, A. Beitlerova, A. Nagura, Y. Shoji, J. Pejchal, Y. Ohashi, Y. Yokota, A. Yoshikawa, Co-doping effects on luminescence and scintillation properties of Ce doped $Lu_3Al_5O_{12}$ scintillator, nuclear instruments and methods in Physics research section a: accelerators, spectrometers, Detect. Assoc. Equip. 782 (2015) 9–12.
[44] K. Kamada, Y. Shoji, V.V. Kochurikhin, A. Nagura, S. Okumura, S. Yamamoto, J.Y. Yeom, S. Kurosawa, J. Pejchal, Y. Yokota, Large size Czochralski growth and scintillation properties of Co-doped, IEEE Trans. Nucl. Sci. 63 (2016) 443–447.
[45] K. Kamada, M. Nikl, S. Kurosawa, A. Beitlerova, A. Nagura, Y. Shoji, J. Pejchal, Y. Ohashi, Y. Yokota, A. Yoshikawa, Alkali earth co-doping effects on luminescence and scintillation properties of Ce doped $Gd_3Al_2Ga_3O_{12}$ scintillator, Opt. Mater. 41 (2015) 63–66.
[46] K. Yang, C.L. Melcher, P.D. Rack, L.A. Eriksson, Effects of calcium codoping on charge traps in LSO: Ce crystals, Ieee Trans. Nucl. Sci. 56 (2009) 2960–2965.
[47] M. Koschan, K. Yang, M. Zhuravleva, C.L. Melcher, A comparison of the effect of $Ca^{2+}$ codoping in cerium doped GSO with that of LSO and YSO, J. Cryst. Growth 352 (2012) 133–136.
[48] Y. Wu, F. Meng, Q. Li, M. Koschan, C.L. Melcher, Role of Ce $^{4+}$ in the scintillation mechanism of codoped $Gd_3Ga_3Al_2O_{12}$: Ce, Phys. Rev. Appl. 2 (2014) 044009.
[49] S. Blahuta, A. Bessiere, B. Viana, P. Dorenbos, V. Ouspenski, Evidence and consequences of Ce in LYSO: Ce, Ca and LYSO: Ce, Mg single crystals for medical imaging applications, IEEE Trans. Nucl. Sci. 60 (2013) 3134–3141.
[50] Y. Wu, J. Luo, M. Nikl, G. Ren, Origin of improved scintillation efficiency in (Lu, Gd) 3 (Ga, Al) $5O_{12}$: Ce multicomponent garnets: an X-ray absorption near edge spectroscopy study, APL Mater. 2 (2014) 012101.
[51] M. Kitaura, K. Kamada, S. Kurosawa, J. Azuma, A. Ohnishi, A. Yamaji, K. Hara, Probing shallow electron traps in cerium-doped $Gd_3Al_2Ga_3O_{12}$ scintillators by UV-induced absorption spectroscopy, Appl. Phys. Express 9 (2016).
[52] M. Kučera, K. Nitsch, M. Nikl, M. Hanuš, S. Daniš, Growth and characterization of YAG and LuAG epitaxial films for scintillation applications, J. Cryst. Growth 312 (2010) 1538–1545.
[53] M. Kucera, P. Prusa, Chapter 5 LPE-grown thin-film scintillators, in: Nanocomposite, Ceramic and Thin Film Scintillators, Pan Stanford Publishing, 2017, pp. 155–226.
[54] M. Kučera, Z. Lučeničová, M. Hanuš, P. Průša, M. Nikl, O. Lalinský, Improved scintillation properties of co-doped GAGG: Ce, Mg epitaxial garnet films, in: ICDIM 2016–19th International Conference on Defects in Insulating Materials, Lyon, France, 2016.
[55] J. Bok, P. Schauer, Apparatus for temperature-dependent cathodoluminescence characterization of materials, Meas. Sci. Technol. 25 (2014) 075601.
[56] P. Schauer, O. Lalinský, Z. Lučeničová, M. Kučera, Multicomponent garnet film scintillators for SEM electron detectors, in: European Microscopy Congress 2016: Proceedings, Wiley-VCH Verlag GmbH & Co. KGaA, 2016.
[57] S. Shionoya, Photoluminescence, in: D.R. Vij (Ed.), Luminescence of Solids, Springer US, Springer Science+Business Media, New York, 1998, pp. 113–114.
[58] R. Autrata, P. Schauer, Cathodoluminescent properties of single crystal materials for electron microscopy, Scanning Microsc. (1995) 1–12. Supplement.